
Article:
Moghaddam, H., Hosseini Gelekolai, S.M. and Hajirasouliha, I. orcid.org/0000-0003-2597-8200 (2018) More efficient lateral load patterns for seismic design of steel moment resisting frames. Proceedings of the Institution of Civil Engineers: Structures and Buildings. Paper 1700064. ISSN 0965-0911

https://doi.org/10.1680/jstbu.17.00064

More Efficient Lateral Load Patterns for Seismic Design of Steel Moment Resisting Frames

Hassan Moghaddam [1], Seyed Mojtaba Hosseini Gelekolai [1] and Iman Hajirasouliha [2*]

[1] *Department of Civil Engineering, Sharif University of Technology, Tehran, Iran*

[2] *Department of Civil & Structural Engineering, the University of Sheffield, Sheffield, UK*

* Corresponding author. E-mail: i.hajirasouliha@sheffield.ac.uk

ABSTRACT:

The preliminary design of building structures is normally based on the equivalent lateral forces provided in seismic design guidelines. The height-wise distribution of these loads is predominantly based on elastic vibration modes. However, as structures exceed their elastic limits in severe earthquakes, these design load patterns may not necessarily lead to efficient distribution of strength within the structures. To address this issue, several alternative load patterns have been proposed for seismic design of nonlinear structures. However, due to the simplifications involved in the development of these design load patterns, their adequacy should be assessed for different structural systems and earthquake excitations before they can be used in common practice. This paper aims to identify the most suitable lateral load patterns for seismic design of steel moment resisting frames. The nonlinear seismic behaviour of 3, 5, 7, 10, and 15-storey frames designed with nine different lateral load patterns are compared under 20 real and synthetic spectrum-compatible earthquakes using performance parameters such as maximum inter-storey drift, maximum plastic hinge rotation and cumulative damage. It is shown that, for the same structural weight, structures designed with more efficient load patterns experience up to 68% less global damage compared to their code-based counterparts.

Keywords: Seismic Engineering, Steel Structures, Buildings Structure & Design

1. INTRODUCTION

The preliminary design of most buildings is normally based on equivalent static forces obtained from seismic design guidelines and codes of practice. The height-wise distribution of these static forces is implicitly based on the dynamic response of elastic structures (Chopra 2012). As structures exceed their elastic limits in severe earthquakes, the use of inertia forces corresponding to the elastic modes may not lead to the best design solutions.

The seismic performance of code-based designed lateral load resisting systems has been widely studied (e.g. Kato and Akiyama 1982; Moghaddam 1996; Mohammadi et al. 2004; Moghaddam and Mohammadi 2006). In the light of these investigations, it was found that the lateral load distribution used by current seismic design guidelines does not always lead to the uniform distribution of ductility demand and damage within the structure. Therefore, the employment of such lateral load patterns does not guarantee the optimal distribution of structural materials throughout the structures in the nonlinear range of behaviour. It was also concluded that a uniform distribution of ductility demands can be obtained by using other lateral design load patterns.

Several researchers have attempted to develop more efficient lateral design load patterns for seismic design of multi-storey buildings. By conducting a trial-and-error dynamic response analyses, Kato and Akiyama (1982) determined the height-wise distribution of maximum storey shear forces of elastoplastic frames to develop uniform plastic deformations under the El Centro 1940 ground motion. They concluded that the shear distribution which leads to a uniform plastic deformation almost coincides with the distribution of maximum storey shear forces under the design earthquake.

By comparison between different lateral load distribution patterns, Moghaddam and Karami-Mohammadi (2006) introduced a new design load pattern for shear-building structures to obtain a more uniform distribution of inter-storey ductility demands. Using a similar approach, Park and Medina (2007) and Motamedi and Nateghi (2008) proposed new lateral design load patterns for seismic design of steel moment-resisting frames based on the concept of uniform damage and uniform earthquake energy distribution, respectively. Lee and Goel (2001) and Chao and Goel (2007) analysed a series of steel moment and braced frames subjected to earthquake excitations. They showed that, in

general, there is a discrepancy between the earthquake induced shear forces and those determined by assuming code-based design load distribution patterns. Based on their results, they suggested a shear distribution factor which was then validated for a wide range of structural systems such as Moment Resisting Frames, Eccentrically-Braced Frames and Special Truss Moment Frames (Goel et al. 2010). However, the effects of ground motion characteristics and the degree of nonlinearity are not directly considered in their suggested design force distribution. In another relevant study, Degochi et al. (2008) proposed a load pattern for seismic design of steel frames using the shear forces developed in an elastic bar with uniform stiffness and mass distributions under a velocity design response spectrum.

Moghaddam and Hajirasouliha (2006) and Moghaddam and Hajirasouliha (2008) developed an effective optimization method based on the concept of uniform damage distribution to find optimum lateral load patterns for seismic design of non-linear shear-building structures. They showed that, for the same target storey-ductility demand, structures that are designed with the optimum load pattern require considerably lower structural weight compared to those designed using conventional methods. In a follow-up study, Hajirasouliha and Moghaddam (2009) proposed a new design load pattern for seismic design of shear buildings that is a function of fundamental period of the structure and the target storey-ductility demand. This load pattern was further developed by Hajirasouliha and Pilakoutas (2012) to include the effects of height-wise irregularity and site soil classifications.

While the design lateral load pattern can play an important role in the seismic performance of structures, the load patterns proposed in the previous studies cannot be used directly in practical design of building structures, as they were mainly based on simple models and/or the utilized seismic records were not compatible with modern building code design spectra (such as EC8 and ASCE/SEI 7-10). To address this issue, this study investigates the efficiency of different design load patterns proposed in the previous studies at improving the seismic performance of 3, 5, 7, 10, and 15-storey steel moment resisting frames (SMRFs) under a wide range of real and synthetic design spectrum-compatible earthquakes. Using different seismic performance criteria, the most suitable design load patterns will be identified for practical design purposes.

2. SEISMIC DESIGN LATERAL LOAD PATTERNS

2.1. Code-compliant lateral load pattern (P-1)

Both Eurocode 8 (EC8, EN 1998-1:2004) and ASCE/SEI 7-10 (2010) use the following equation to calculate the lateral seismic force (F_i) at each storey level:

$$F_i = \frac{w_i {h_i}^k}{\sum_{j=1}^{n} w_j {h_j}^k} V; \quad i = 1, 2, \dots, n; \quad k = \begin{cases} 1 & ; \ T \leq 0.5 \\ 0.5T + 0.75 \ or \ 2 & ; 0.5 < T < 2.5 \\ 2 & ; \ T \geq 2.5 \end{cases} \tag{1}$$

where w_i is the weight of the structure at i^{th} level, h_i is the height from the base to level i, n is the total number of storeys, V is the design lateral force at the base of the structure (base shear), k is an exponent related to the structure period, and T is the fundamental period of the structure.

2.2. Lateral load pattern proposed by Goel et al. (P-2)

Goel et al. (2010) proposed the following load pattern for seismic design of structures:

$$F_i = C_{iv} V$$

$$C_{iv} = (\beta_i - \beta_{i+1}) \left(\frac{w_n h_n}{\sum_{j=1}^{n} w_j h_j} \right)^{\alpha T^{-0.2}} ; \quad \beta_{n+1} = 0 \tag{2}$$

$$\beta_i = \frac{V_i}{V_n} = \left(\frac{\sum_{j=i}^{n} w_j h_j}{w_n h_n} \right)^{\alpha T^{-0.2}} ; \quad i = 1, 2, \dots, n$$

where β_i and V_i are the shear distribution factor and the storey shear force at level i, respectively. The parameter α was originally proposed as 0.5 by Lee and Goel (2001), which was later modified to 0.75 by considering a wider range of steel framing systems (Goel et al., 2010).

2.3. Lateral load pattern proposed by Hajirasouliha and Moghaddam (P-3)

The load pattern suggested by Hajirasouliha and Moghaddam (2009) and Hajirasouliha and Pilakoutas (2012) can be expressed as follows:

$$F_i = \frac{w_i \phi_i}{\sum_{j=1}^{n} w_j \phi_j} V; \quad \phi_i = (a_i T + b_i) \mu_T^{\frac{c_i T + d_i}{100}}; \quad i = 1, 2, \dots, n \tag{3}$$

where μ_T is the target ductility demand, and a_i, b_i, c_i, d_i are constant coefficients at level i that can be calculated for each set of design earthquakes. The constant coefficients corresponding to different soil profiles are given in Hajirasouliha and Pilakoutas (2012) as a function of relative height.

2.4. Lateral load pattern proposed by Park and Medina (P-4)

The lateral load pattern proposed by Park and Medina (2007) for regular steel moment-resisting frames is given by the following formula:

$$F_i = \left(\frac{\left(1-\frac{F_t}{V_y}\right) w_i {h_i}^k}{\sum_{j=1}^{n} w_j {h_j}^k} + \delta_{in} \frac{F_t}{V_y} \right) V_y; \quad i = 1, 2, \ldots, n; \quad \delta_{in} = \begin{cases} 0; & if\ i \neq n \\ 1; & if\ i = n \end{cases}$$

$$k = 0.56 - 0.17\mu_T; \quad 1 \leq \mu_T \leq 5 \tag{4}$$

$$\frac{F_t}{V_y} = 0.32 - 0.0016H - 0.13k; \quad 22m \leq H \leq 66m$$

where F_t is a concentrated force at the top of the structure, w_i is the weight at level i, and V_y is the base shear strength to achieve a specified target storey ductility ratio of μ_T. H is the total height of the structure from the base.

2.5. Lateral load pattern proposed by Building Center of Japan (P-5)

The seismic code of Japan (BCJ, 1997) suggests the following shear strength distribution pattern:

$$V_{yi} = C_B A_i \alpha_i W_t; \quad \alpha_i = \frac{W_i}{W_t}; \quad A_i = 1 + \left(\frac{1}{\sqrt{\alpha_i}} - \alpha_i \right) \frac{2T}{1+3T}; \quad T = 0.03H \tag{5}$$

where V_{yi} is the shear strength of the i[th] storey, C_B is the base shear coefficient, A_i is the shear coefficient distribution which represents the vertical distribution of the seismic load, and W_t is the total weight of the structure.

2.6. Lateral load pattern proposed by Deguchi et al. (P-6)

Deguchi et al. (2008) proposed the following storey shear strength distribution for seismic design of steel frames:

$$V_{yi} = C_B A_i \alpha_i W_t; \quad \alpha_i = \frac{W_i}{W_t}; \quad A_i = \frac{1}{\sqrt{\alpha_i}} \tag{6}$$

All parameters are defined in previous equations.

2.7. Lateral load pattern proposed by Kato et al. (P-7)

The following load pattern is suggested by Kato et al. (1982) for elastoplastic frames:

$$V_{yi} = C_B A_i \alpha_i W_t; \quad \alpha_i = \frac{W_i}{W_t}$$

$$A_i = 1 + 1.5927\xi_i - 11.8519{\xi_i}^2 + 42.5833{\xi_i}^3 - 59.4827{\xi_i}^4 + 30.1586{\xi_i}^5 \tag{7}$$

$$\xi_i = 1 - \alpha_i$$

2.8. Lateral load pattern proposed by Motamedi and Nateghi (P-8)

Motamedi and Nateghi (2008) proposed the following a triangular-rectangular load pattern for seismic design of steel moment-resisting frames:

$$F_i = \begin{cases} B' & if\ i \le n/2 \\ \frac{2iB'}{n} & if\ i > n/2 \end{cases} ;\ B' = \frac{4V_y}{3H} \quad ; \quad i = 1, 2, \dots, n \tag{8}$$

In the above equation, B' is equal to $\frac{2b}{3}$, where b is the altitude of the triangular load in Iranian seismic code (BHRC, 2005).

2.9. Lateral load pattern proposed by Moghaddam and Karami Mohammadi (P-9)

Moghaddam and Karami Mohammadi (2006) load pattern is defined as a concentrated load at the top level (F_t) accompanied by uniform distribution of the rest of base shear (V) along the height of the structure:

$$F_i = \frac{1}{n}(V - F_t) + \delta_{in}\, F_t; \quad i = 1, 2, \dots, n; \quad \delta_{in} = \begin{cases} 0; & if\ i \ne n \\ 1; & if\ i = n \end{cases}$$

$$F_t = \vartheta T V \tag{9}$$

$$\vartheta = (0.9 - 0.04\mu_T)e^{-(0.6+0.03\mu_T)T}$$

3. MODELLING AND ASSUMPTIONS

3.1. Case Study Frames

To investigate the efficiency of different seismic design load patterns, 3, 5, 7, 10, and 15-storey ordinary moment resisting frames (with the typical geometry shown in Figure 1) were examined. The bay-width and the storey-height of the frames were 6 m and 3 m, respectively, and all supports were considered to be fixed. The uniformly distributed dead and live loads were assumed as 6 kN/m^2 and 2 kN/m^2 for interior stories, and 6 kN/m^2 and 1.5 kN/m^2 for the roof level, respectively. The frames were assumed to be located on a soil type D category of ASCE/SEI 7-10, with the design spectral response acceleration at short periods and 1-sec period equal to 0.40g and 0.64g, respectively (see Figure 2). The structural elements were designed to support gravity loads and lateral loads in accordance with the minimum requirements of ANSI/AISC 360-10. The P-Delta affects were taken into account in the

129 design process of the MRFs. The seismic force-resisting system was considered to be steel
130 intermediate moment frame with the response modification coefficient (R) and overstrength factor
131 (Ω_0) equal to 4.5 and 3, respectively. The yielding stress and Young's modulus of the steel material
132 were taken to be 235.4 MPa and 200 GPa, respectively. Strain hardening of steel was taken into
133 account by considering the tangent modulus E_T equal to E/50, where E is the modulus of elasticity of
134 steel material (Mazzolani and Gioncu 1995).

135 IPB and IPE sections, according to DIN-1025 (1995) standard, were chosen for columns and
136 beams, respectively. To obtain the best design solutions, conceptual auxiliary sections were artificially
137 developed by assuming a continuous variation of section properties. The optimum size of each
138 structural element was calculated based on the required capacity under the design loads. For example,
139 Table 1 shows the show the beam and column cross sections of the 5-storey frames designed based on
140 the nine different load patterns. The numbers in this table show the area of the sections in cm^2.

141 In this study, the drift limitations suggested by the design guidelines (e.g. EC8 and ASCE/SEI 7-
142 10) were not controlled during the design process in order to provide a fair means of comparison
143 between different load patterns using the same amount of structural weight. While the effects of
144 uncertainties on the seismic performance of the structures is not in the scope of this paper, previous
145 studies by Hajirasouliha et al. (2016) showed that typical uncertainties in conventional steel frames do
146 not significantly influence the efficiency of the optimum design frames.

147 Nonlinear time history analyses were conducted using OpenSees (2015). The Rayleigh damping
148 model with a constant damping ratio of 0.05 was assigned to the first mode and to the modes at which
149 the cumulative mass participation exceeds 95%. A distributed plasticity fibre-based model in
150 OpenSees (2015) was employed to model the nonlinear behaviour of the beam and column elements.
151 The model can take into account the change in the plastic hinge length and variation of the stiffness
152 under single or double curvature conditions. The P-Delta second order effects were also included in
153 the non-linear dynamic analyses. The contribution of the panel zone deformation was considered to be
154 insignificant in the MRFs with rigid connections (Mazzolani and Gioncu 2000; Medina and
155 Krawinkler 2005).

Figs-1-2

Table 1. Beam and column cross sections of the 5-storey frames designed based on the nine different load patterns (numbers are the area of the sections in cm^2).

Section		P-1	P-2	P-3	P-4	P-5	P-6	P-7	P-8	P-9
1st Floor	C11	IPB 149	IPB 149	IPB 147	IPB 142	IPB 148	IPB 147	IPB 147	IPB 147	IPB 146
	C12	IPB 264	IPB 253	IPB 275	IPB 305	IPB 272	IPB 264	IPB 270	IPB 285	IPB 272
	C13	IPB 157	IPB 152	IPB 156	IPB 162	IPB 155	IPB 152	IPB 153	IPB 162	IPB 152
	B11	IPE 115	IPE 113	IPE 114	IPE 113	IPE 114	IPE 112	IPE 113	IPE 115	IPE 112
	B12	IPE 110	IPE 109	IPE 109	IPE 111	IPE 109	IPE 108	IPE 108	IPE 111	IPE 106
	B13	IPE 97	IPE 95	IPE 97	IPE 98	IPE 96	IPE 95	IPE 95	IPE 99	IPE 95
2nd Floor	C21	IPB 118	IPB 124	IPB 116	IPB 110	IPB 117	IPB 122	IPB 120	IPB 113	IPB 119
	C22	IPB 167	IPB 165	IPB 162	IPB 157	IPB 162	IPB 161	IPB 162	IPB 163	IPB 158
	C23	IPB 133	IPB 135	IPB 131	IPB 126	IPB 132	IPB 133	IPB 132	IPB 128	IPB 132
	B21	IPE 106	IPE 107	IPE 105	IPE 104	IPE 105	IPE 105	IPE 105	IPE 105	IPE 105
	B22	IPE 104	IPE 102	IPE 102	IPE 99	IPE 102	IPE 101	IPE 101	IPE 101	IPE 99
	B23	IPE 94	IPE 92	IPE 93	IPE 96	IPE 93	IPE 92	IPE 92	IPE 96	IPE 92
3rd Floor	C31	IPB 84	IPB 86	IPB 83	IPB 79	IPB 84	IPB 85	IPB 84	IPB 81	IPB 84
	C32	IPB 132	IPB 131	IPB 134	IPB 141	IPB 134	IPB 131	IPB 131	IPB 138	IPB 132
	C33	IPB 112	IPB 112	IPB 111	IPB 110	IPB 111	IPB 110	IPB 109	IPB 111	IPB 107
	B31	IPE 101	IPE 101	IPE 99	IPE 93	IPE 100	IPE 100	IPE 99	IPE 98	IPE 99
	B32	IPE 94	IPE 93	IPE 94	IPE 94	IPE 94	IPE 93	IPE 93	IPE 95	IPE 93
	B33	IPE 92	IPE 92	IPE 92	IPE 92	IPE 92	IPE 92	IPE 92	IPE 92	IPE 92
4th Floor	C41	IPB 75	IPB 75	IPB 75	IPB 75	IPB 75	IPB 75	IPB 75	IPB 75	IPB 75
	C42	IPB 86	IPB 101	IPB 86	IPB 77	IPB 89	IPB 102	IPB 98	IPB 77	IPB 98
	C43	IPB 113	IPB 113	IPB 109	IPB 96	IPB 110	IPB 111	IPB 112	IPB 101	IPB 107
	B41	IPE 90	IPE 95	IPE 90	IPE 88	IPE 91	IPE 95	IPE 93	IPE 88	IPE 93
	B42	IPE 93	IPE 93	IPE 94	IPE 94	IPE 94	IPE 93	IPE 93	IPE 94	IPE 94
	B43	IPE 92	IPE 92	IPE 92	IPE 92	IPE 92	IPE 92	IPE 92	IPE 92	IPE 92
5th Floor	C51	IPB 69	IPB 67	IPB 70	IPB 53	IPB 69	IPB 67	IPB 66	IPB 62	IPB 67
	C52	IPB 79	IPB 80	IPB 79	IPB 77	IPB 78	IPB 79	IPB 78	IPB 77	IPB 78
	C53	IPB 44	IPB 51	IPB 45	IPB 40	IPB 45	IPB 52	IPB 48	IPB 43	IPB 62
	B51	IPE 78	IPE 83	IPE 78	IPE 77	IPE 79	IPE 83	IPE 82	IPE 77	IPE 82
	B52	IPE 89	IPE 88	IPE 89	IPE 90	IPE 89	IPE 88	IPE 88	IPE 90	IPE 88
	B53	IPE 87	IPE 86	IPE 87	IPE 85	IPE 86	IPE 86	IPE 86	IPE 86	IPE 85

3.2. Selected Ground Motions

Five medium-to-strong natural ground motion records were selected from PEER ground motion database (PEER, 2010) as listed in Table 2. All of these ground motions correspond to soil class D of ASCE/SEI 7-10 and are recorded in low to moderate distances from the epicentre (less than 45 km) with high local magnitudes (i.e. M>6.7). On average, the selected ground motions provide a reasonably close approximation to the design response spectra of ASCE/SEI 7-10 for the site class D

in high seismic zones (i.e. PGA=0.4g), especially at the first mode periods of the designed frames. Therefore, in this study these earthquake records were used directly without being normalized (Nabid et al. 2017). The acceleration spectrum of these ground motions are compared with ASCE/SEI 7-10 design spectrum in Figure 2.

Fifteen synthetic records were also generated using SIMQKE program (Vanmarke, 1976) to be compatible with the soil type C of ASCE/SEI 7-10 design spectrum. Figure 2 demonstrates a good compatibility between the average of these synthetic earthquakes and the code design spectrum. Therefore, these synthetic earthquakes can be considered to be representatives of the response spectrum used in the design process.

Table 2. Characteristics of the selected ground motions

No.	Earthquake	Record/ Component	Station	Magnitude (Ms)	PGA (g)	PGV (cm/s)	PGD (cm)
1	Duzce, Turkey 1999	DUZCE/ DZC270	Duzce	7.3	0.535	83.5	51.59
2	Imperial Valley 1979	IMPVALL/ HE04140	955 El Centro Array #4	6.9	0.485	37.4	20.23
3	Loma Prieta 1989	LOMAP/ G03000	47381 Gilroy Array #3	7.1	0.555	35.7	8.21
4	Cape Mendocino 1992	CAPEMEND/ PET090	89156 Petrolia	7.1	0.662	89.7	29.55
5	Northridge 1994	NORTHR/ NWH360	24279 Newhall - Fire Sta	6.7	0.59	97.2	38.05

3.3. Design Load Patterns

The 3, 5, 7, 10, and 15-storey moment resisting frames were designed using the nine different load patterns discussed in section 2 (45 frames in total). For the frames designed with the load patterns P-2 to P-9, the sum of inter-storey shear forces was scaled so that the total structural weight becomes equal to that of the reference models designed with ASCE load pattern (P-1). By using this adjustment, the fundamental period of the frames designed with different load patterns were very close to the fundamental period of the corresponding ASCE frame.

While almost all of the proposed load patterns depend on the fundamental period of the structure T, load patterns P-3, P-4 and P-9 are also a function of the target ductility demand μ_T. Calculating these load patterns is not straightforward as T and μ_T are also affected by the seismic design loads.

Therefore, in this study an iterative method was used to update the values of T and μ_T for more accurate calculation of the seismic design loads. In the first step, the target ductility demand was considered to be 2 and the fundamental period of the structure was calculated based on the ASCE suggested equation. Subsequently, the structure was designed based on the calculated loads and the accurate fundamental period was obtained from the FE model. If the target ductility is also required to calculate the design load pattern, the structure was subjected to the 15 synthetic spectrum-compatible earthquakes and the average storey ductility (maximum displacement of each storey divided by the yield displacement of the storey) was calculated. The yield displacements were obtained from a non-linear pushover analysis (Hajirasouliha and Doostan, 2009). The iteration process was repeated until the difference between T and μ_T values in two subsequent steps became negligible. For example, Figure 3 shows the lateral load patterns obtained for the seismic design of the 10-storey frame.

It is shown in Figure 4(a) that the models designed with different load patterns have similar total structural weight, while their design base shear can be very different. In general, for high-rise buildings (10 and 15 storey) the design load patterns P-3 and P-9 led to maximum base shear, while P-1 and P-2 resulted in lower design base shear values compared to the other load patterns (see Figure 4(b)). For low- to medium-rise buildings, the design load pattern P-4 led to the highest base shear values.

Figs-3-4

4. ADEQUACY OF THE DESIGN LOAD PATTERNS

In this study, the following performance parameters were used to identify the most suitable design load patterns for SMRFs with different number of storeys.

4.1. Inter-Storey Drift

Maximum inter-storey drift has been widely used to evaluate the level of damage to both structural and non-structural elements in building structures. ASCE 41-13 (2013) limits the maximum inter-storey drift ratio to 0.7%, 2.5% and 5% for immediate occupancy (IO), life safety (LS) and collapse prevention (CP) performance levels, respectively. Figure 5 compares the average of the inter-storey drift ratios in the 15 synthetic earthquakes spectrum-compatible earthquakes for the 3, 5, 7, 10 and 15-storey frames designed with different load patterns (675 different cases in total). The results indicate that the design lateral load pattern can play an important role in controlling the maximum inter-storey drift and also some design load patterns can be considerably more efficient than the conventional code-compliant lateral loads.

It is shown in Figure 5 that, for the same structural weight, the load patterns P-2, P-6 and P-7 in general led to the design solutions with lower maximum inter-storey drift ratios compared to the other load patterns. While the load pattern P-4 could not control the maximum inter-storey drift ratios at the top floors of low to medium rise buildings (3, 5 and 7-stroey frames), it was considerably more efficient for high-rise buildings (10 and 15-storey frames). The load pattern P-8 resulted in structures with high maximum inter-storey drift ratios in the top floors, especially in high-rise buildings.

Fig-5

It is shown in Figure 5 that the top floors of SMRFs usually exhibit higher inter-storey drift ratios when compared to the bottom floors. Also it can be noted that in general the maximum inter-storey drift distribution of low-rise buildings follow the first mode shape of the structure, while for the high-rise buildings the effect of higher modes is evident. The effect of higher modes is especially dominant when the design load patterns P-4 and P-8 are utilized.

For better comparison, Table 3 presents the maximum inter-storey drift ratio and the performance limit of the frames designed with different load patterns (average of 15 synthetic earthquakes). It is shown that the SMRFs designed with the code suggested load pattern (P-1) always satisfied the collapse prevention (CP) performance level under the design earthquakes, while using P-4 and P-8

241 design load patterns led to the structural collapse in low to medium-rise and high-rise buildings,
242 respectively. For the same structural weigh, structures designed based on P-2, P-6 and P-7 remained in
243 the life safety (LS) performance level, which confirms the efficiency of these load patterns. The results
244 in Table 3 also indicate that the design load pattern P-2 suggested by Goel et al. (2010) was the most
245 efficient pattern to control maximum inter-storey drifts in almost all cases.

246

247 **Table 3.** Maximum inter-storey drift ratio and performance limit of the SMRFs designed with different
248 load patterns (average of 15 synthetic earthquakes)

Design Load Pattern	3- Storey		5- Storey		7-Storey		10-Storey		15-Storey	
	Drift Ratio (%)	Performance Level	Drift Ratio (%)	Performance Level	Drift Ratio (%)	Performance Level	Drift Ratio (%)	Performance Level	Drift Ratio (%)	Performance Level
P-1	2.73	CP	2.78	CP	3.30	CP	3.58	CP	3.95	CP
P-2	1.93	LS	1.73	LS	1.90	LS	2.15	LS	2.28	LS
P-3	2.55	CP	2.50	LS	3.20	CP	3.53	CP	4.20	CP
P-4	5.15	Collapse	5.10	Collapse	5.20	Collapse	2.38	LS	2.28	LS
P-5	2.85	CP	2.35	LS	2.50	LS	2.68	CP	2.88	CP
P-6	2.00	LS	1.93	LS	2.00	LS	2.18	LS	2.25	LS
P-7	2.15	LS	1.88	LS	2.20	LS	2.45	LS	2.50	LS
P-8	3.60	CP	4.13	CP	4.30	CP	4.95	CP	5.50	Collapse
P-9	2.15	LS	2.15	LS	2.23	LS	2.53	CP	3.00	CP

249

250 ***4.2. Plastic Hinge Rotation***

251 To evaluate the seismic performance of the frames, the maximum plastic rotation of each beam and
252 column element (Θ_{pi}) was compared with the allowable plastic rotation (Θ_{all}) under the design
253 earthquake. In this study, Θ_{all} was assumed to be the maximum allowable rotation of each element in
254 life safety (LS) performance level specified in ASCE41-13 (2013). For steel beams, Θ_{all} is a function
255 of the yield rotation (Θ_y) and the section dimensions, while for steel columns the maximum axial force
256 of the column is also considered. According to ASCE41-13 (2013), the yield rotation of beam and
257 column elements can be calculated by using Equations 9 and 10, respectively.

$$\theta_{yb} = \frac{ZF_{ye}l_b}{6EI_b} \tag{9}$$

$$\theta_{yc} = \frac{ZF_{ye}l_c}{6EI_c}(1 - \frac{P}{P_{ye}}) \quad (10)$$

where E and F_{ye} are the elastic modulus of the material and the expected yield stress. I_b, l_b, and I_c, l_c represent the moment of inertia and the effective length of the beam and column elements, respectively. Z is the plastic modulus of each cross-section, and P and P_{ye} denote the axial force of the column and the expected axial yield force of the column, respectively.

The Θ_p/Θ_{all} ratio was calculated for all structural elements of the 3, 5, 7, 10 and 15-storey frames designed with different load patterns. Figure 6 compares the maximum and the average of the results in the 15 synthetic spectrum-compatible earthquakes. Overall, the maximum Θ_p/Θ_{all} ratios (in Figure 6 (a)) are in good agreement with the performance levels obtained based on the inter-storey drift ratios (in Table 3). It is shown that load patterns P-2, P-6 and P-7 in general provided the best design solutions with lower Max Θ_p/Θ_{all} ratios. In most cases, these three load patterns led to lower Mean Θ_p/Θ_{all} ratios as well, which implies they could efficiently reduce the overall displacement demands of the designed structures. It is clear from Figure 6 (a) that using the load pattern P-8 resulted in very high plastic rotations in the structures with more than 5 storeys. As shown in Figure 5, it is mainly due to the soft storey failure of the top floors. However, this design load patterns seems to be acceptable for 3 and 5-storey buildings.

Fig-6

To provide more details on the height-wise inter-storey drift distributions ratios, Figure 7 (a) compares the "average", "average + standard deviation" and "average – standard deviation" of the results of the 5-storey frame under the 15 synthetic spectrum-compatible earthquakes. The results indicate that the average values could efficiently show the general trend of the results in the individual earthquakes. For better comparisons, the probability density of the maximum inter-storey drifts at different storey levels are also calculated as depicted in Figure 7 (b). It is shown that, in general, the

utilised records led to maximum inter-storey drift ratios with a relatively wide normal distribution at all storey levels.

Fig-7

4.3. Cumulative damage

To investigate the extent of damage within the designed structures, the damage index proposed by Baik et al. (1988) based on the classical low-cycle fatigue approach is used in this study (Equation 11). The inter-storey inelastic deformation is chosen as the basic damage quantity, and the cumulative damage index after N cycles of plastic deformation is calculated as:

$$D_i = \sum_{j=1}^{N} \left(\frac{\Delta \delta_{pj}}{\delta_{yi}} \right)^c \tag{11}$$

where D_i is the cumulative damage index at ith storey, ranging from 0 for undamaged to 1 for severely damaged storeys. N is the number of plastic excursions. $\Delta\delta_{pj}$ and δ_{yi} denote the plastic deformation of ith storey in jth cycle and the nominal yield deformation of ith storey, respectively. c is a parameter to account for the plastic deformation magnitude which is taken to be 1.5 as suggested by Krawinkler and Zohrei (1984).

To evaluate the total damage of the structure, the global damage index D_t was calculated as a weighted average of the damage indices at the storey levels by using the dissipated energy as the weighting function:

$$D_t = \frac{\sum_{j=1}^{n} D_i W_{pi}}{\sum_{j=1}^{n} W_{pi}} \tag{12}$$

In the above equation, W_{pi} and D_i are the dissipated energy and the damage index at ith storey, respectively, and n is the total number of storeys. The global damage index D_t was calculated for the designed 3, 5, 7, 10 and 15-storey frames under the 15 synthetic spectrum-compatible earthquakes. For example, Figure 8 shows the global damage index D_t of the 5-stroey frames designed with different

304 load patterns under the synthetic spectrum-compatible earthquakes number 4, 8 and 12. While there
305 are some discrepancy between the global damage indices in different synthetic earthquakes, the results
306 show a very similar trend. Therefore, the average of the results can provide reliable information to
307 assess the efficiency of each design load pattern.

308

309 Fig-8

310

311 Figure 9 compares the average of the results in 15 synthetic earthquakes for the 3, 5, 7, 10 and 15-
312 storey frames designed with the nine different load patterns. It should be mentioned that the damage
313 indices above 1 represent extensive damage and failure of the structure.

314 In general, the global damage results are in very good agreement with the maximum inter-storey
315 drift ratios and performance limits discussed in previous sections (e.g. Table 3). It is shown in Figure 9
316 that the load patterns P-2, P-6 and P-7 led to design solutions with lower global indices compared to
317 the other load patents. The load patterns P-5 and P-9 could also control the global damage of the
318 structures with different number of storeys within an acceptable range. However, the load patterns P-3
319 and P-4 were suitable only for low to mid-rise structures (less than 7 storeys) and high-rise structures
320 (more than 10 storeys), respectively. Using the load pattern P-8 resulted in high global damage indices
321 especially in high-rise buildings, which confirms the previous conclusion that this load pattern is not
322 suitable for seismic design of SMRFs. Also it can be noted from Figure 9 that the efficiency of the
323 EC8 and ASCE/SEI 7-10 design load distribution pattern (P-1) decreases by increasing the number
324 storeys. This can be due to the fact that the code-based design patterns cannot accurately take into
325 account the higher mode effects in non-linear multi-storey structures under strong earthquakes as was
326 also reported by Hajirasouliha and Moghaddam (2009) and Hajirasouliha and Pilakoutas (2012).

327 By calculating the average of the results for the 3, 5, 7, 10 and 15-storey frames (red dotted line in
328 Figure 9), it can be concluded that, for the same structural weight, structures designed with the load
329 patterns P-2, P-6 and P-7 on average exhibit 68%, 66% and 54% less structural damage compared to

their code-based counterparts. This implies that the seismic performance of the non-linear SMRFs can be significantly improved by using more appropriate design load patterns.

Fig-9

5. EFFECT OF EARTHQUAKE EXCITATION

To investigate the efficiency of different design load patterns under real earthquake excitations, the designed frames were also subjected to the five selected strong earthquake records listed in Table 2. Overall, the results confirmed the general conclusions made based on the synthetic spectrum-compatible earthquakes in previous sections. For example, Figures 10 and 11 compare the maximum inter-storey drift distribution and the global damage index of 5-storey frames designed with different load patterns under the 15 synthetic and the 5 selected earthquake records. It is shown that, on average, the global damage indices and the maximum inter-storey drift ratios corresponding to different design load patterns exhibit a very similar trend in real and synthetic earthquake records. For example, in both cases the load patterns P-2, P-6 and P-7 provided the best design solutions with minimum global damage and inter-storey drift ratios, while using the load patterns P-4 and P-8 led to a very poor seismic performance. Therefore, it can be concluded that the general results based on the average of synthetic spectrum-compatible earthquakes are also valid for real earthquake records.

Figs-10-11

6. DESIGN VERSUS INDUCED SEISMIC FORCES

In general, lateral seismic design load patterns aim to represent the height-wise distribution of maximum storey shear forces during design earthquakes. Hence, the agreement between the design and the induced storey shear forces can be used as a measure to assess the adequacy of each seismic design load pattern. In this section, the relative distribution of design storey shear forces $(V_i/V_n)_D$ in 3,

5, 7, 10, and 15-storey frames designed with different load patterns are compared with the average relative distribution of maximum storey shear forces $(V_i/V_n)_E$ occurred during the 15 synthetic spectrum-compatible earthquakes. Figure 12 shows the results for the load patterns P-1 to P-9. For a better comparison, the mean absolute error (MAE) between $(V_i/V_n)_D$ and $(V_i/V_n)_E$ ratios are also calculated for each design load pattern by using the following equation:

$$MEA = \frac{1}{n}\sum_{i=1}^{n}\left|\left(\frac{V_i}{V_n}\right)_D - \left(\frac{V_i}{V_n}\right)_E\right| \quad (13)$$

The *MEA* factor would tend to zero if the height-wise distribution of the storey shear forces used during the design process is similar to the average distribution of maximum storey shear forces under the design spectrum-compatible earthquakes. Figure 13 compares the *MEA* factor for the frames designed with different load patterns. In general, the *MEA* results follow a similar trend as the global damage indices, and the design load patterns with lower damage indices (i.e. P-2, P-6 and P-7) show a better agreement with the maximum storey shear forces observed during the design earthquakes.

Figs-12-13

It should be mentioned that the selected seismic design load pattern can have a significant effect on the sizing of the structural members, which in turn affects the dynamic characteristics of the structural system both in the linear and nonlinear regions. Therefore, the maximum storey shear forces that are exhibited by the structure during design earthquakes may not represent the best design lateral load pattern as it was shown in previous studies (e.g. Moghaddam 1996, Hajirasouliha and Moghaddam 2009). However, it is shown in this paper that this criterion can be used to assess the overall adequacy of the selected design load pattern, as the results are in agreement with other performance parameters such as maximum inter-storey drift, plastic hinge rotation and global damage.

In this study, the average response of each group of earthquakes was used to evaluate the seismic performance of the moment resisting frames. While 84th, 50th and 16th percentiles of the results (as suggested by Longo et al. 2009; Tenchini et al. 2014; and Silva et al. 2016) can be also used to provide

more in-depth information, this will not affect the general conclusions of this article. In general, the outcomes of this study should provide very helpful information for structural designers, especially those involved in the seismic design of buildings, to obtain more efficient and resilient multi-storey steel moment resisting frames suitable for seismic regions.

6. CONCLUSIONS

An extensive analytical study was conducted to investigate the effects of lateral design load pattern on the seismic performance of SMRFs. The nonlinear seismic behaviour of 3, 5, 7, 10, and 15-storey frames designed with nine different design load patterns (from design guidelines and literature) were compared under 15 synthetic spectrum-compatible earthquakes and 5 real strong earthquake ground motions. Different performance parameters such as maximum inter-storey drift, plastic hinge rotation and cumulative damage were used to identify the most suitable load patterns for practical applications. Based on the results presented in this paper, the following conclusions can be drawn:

- Overall, the efficiency of Eurocode 8 (EC8, EN 1998-1:2004) and ASCE/SEI 7-10 (2010) lateral design load pattern decreases by increasing the number of storeys. This may imply that the code suggested load pattern cannot accurately take into account the higher mode effects in non-linear multi-storey frames under strong earthquakes. The design load pattern proposed by Moghaddam and Karami Mohammadi (2006) and the seismic code of Japan (BCJ, 1997), on average, led to the design solutions with slightly lower global damage indices compared to Eurocode 8 (EC8, EN 1998-1:2004) and ASCE/SEI 7-10 (2010).
- The Park and Medina (2007) proposed load pattern could not control the maximum inter-storey drift ratios at the top floors of low to medium-rise SMRFs, which led to very high global damage indices and collapse in these structures. However, this load pattern could provide acceptable design solutions for high-rise buildings. In contrast, the Hajirasouliha and Moghaddam (2009) proposed pattern was only suitable for low to medium-rise buildings. The load pattern proposed by Motamedi and Nateghi (2008) was shown to be inappropriate in most cases.

- The SMRFs designed with the load patterns proposed by Goel et al. (2010), Deguchi et al. (2008) and Kato et al. (1982) exhibited considerably (up to 68%) lower inter-storey drift ratios, plastic hinge rotations and global damage indices compared to their code-based counterparts with the same structural weight. While all of these load patterns are suitable for the seismic design of SMRFs, the Goel et al. (2010) load pattern seems to be the most efficient one.
- It was shown that the storey shear distribution of the design load patterns with better seismic performance had a better agreement with the distribution of maximum storey shear forces during the design earthquakes. Therefore, this criterion can be used as a simple measure to assess the adequacy of the design load pattern in practice.

REFERENCES

AISC (American Institute of Steel Construction) (2010) ANSI/AISC 360-10: Specification for structural steel buildings. American Institute of Steel Construction, Chicago, IL, USA.

ASCE (American Society of Civil Engineers) (2010) ASCE/SEI 07-10: Minimum design loads for buildings and other structures. American Society of Civil Engineers, Virginia, USA

ASCE (American Society of Civil Engineers) (2013) ASCE/SEI41-13: Seismic rehabilitation of existing buildings. American Society of Civil Engineers, Virginia, USA

BCJ (Building Center of Japan) (1997) BCJ: Seismic provisions for design of building structures. Building Center of Japan, Tokyo, Japan.

BHRC (Building and Housing Research Center) (2005) standard No.2800: Iranian code of practice for seismic resistant design of buildings 3rd ed. Building and Housing Research Center, Tehran, Iran.

CEN (Comité Européen de Normalisation) (2004) EN 1998-1:2004 Eurocode 8: Design of structures for earthquake resistance part 1: general rules, seismic actions and rules for buildings. Comité Européen de Normalisation, Lausanne, Switzerland.

Chao SH and Goel SC (2007) A seismic design lateral force distribution based on inelastic state of structures. Earthquake Spectra 23(3): 547-569.

435 Chopra AK (2012) Dynamics of Structures: Theory and Applications to Earthquake Engineering, 4th
436 ed. Prentice Hall Inc., London, UK.

437 Deguchi Y, Kawashima T, Yamanari M and Ogawa K (2008) Seismic design load distribution in steel
438 frame. In *14th World Conference on Earthquake Engineering*, Beijing, China.

439 DIN (Deutsches Institut Fur Normung EV) (1995) DIN 1025: Hot rolled I and H sections:
440 Dimensions, mass and static parameters. Deutsches Institut Fur Normung EV, Berlin, Germany.

441 Goel SC, Liao WC, Bayat MR and Chao SH (2010) Performance-based plastic design (PBPD) method
442 for earthquake-resistant structures: an overview. The Structural Design of Tall and Special
443 Buildings, 19(1): 115-137.

444 Hajirasouliha I and Doostan A (2009) A simplified model for seismic response prediction of
445 concentrically braced frames. Advances in Engineering Software 41(3): 497-505.

446 Hajirasouliha I and Moghaddam H (2009) New lateral force distribution for seismic design of
447 structures. Journal of Structural Engineering ASCE 135(8): 906-915.

448 Hajirasouliha I and Pilakoutas K (2012) Optimum general seismic load distribution for optimum
449 performance-based design of shear-buildings. Journal of Earthquake Engineering 16(4): 443-462.

450 Hajirasouliha I, Pilakoutas K and Mohammadi RK (2016) Effects of uncertainties on seismic
451 behaviour of optimum designed braced steel frames. Steel and Composite Structures 20(2): 317-
452 335.

453 Karami Mohammadi R, El Naggar MH and Moghaddam H (2004) Optimum strength distribution for
454 seismic resistant shear-buildings. International Journal of Solids and Structures 41(22): 6597-
455 6612.

456 Kato B and Akiyama H (1982) Seismic design of steel buildings. Journal of the Structural Division
457 ASCE 108(8): 1709-1721.

458 Lee SS and Goel SC (2001) Performance based design of structures using target drift and yield
459 mechanism. In *Advanced Stability and Seismicity Concept for Performance-Based Design of Steel*
460 *and Composite Structures*, Kyoto, Japan.

461 Longo A, Montuori R, Piluso V (2009) Seismic reliability of Chevron braced frames with innovative
462 concept of bracing members. Adv Steel Constr 5 (4):367-89.

463 Mazzolani FM and Gioncu V (1995) Behaviour of Steel Structures in Seismic Areas, 1st Edition,
464 University Press, Cambridge.

465 Mazzolani FM and Gioncu V (2000) Seismic Resistant Steel Structures, Springer- Verlag Wein, New
466 York.

467 Medina RA and Krawinkler H (2005) Strength demand issues relevant for the seismic design of
468 moment-resisting frames, Earthquake Spectra 21 (2): 415-439.

469 Moghaddam H (1996) Earthquake Engineering, 1st ed. RTRC, Tehran, Iran.

470 Moghaddam H and Hajirasouliha I (2006) Toward more rational criteria for determination of design
471 earthquake forces. International Journal of Solids and Structures 43(9): 2631-2645.

472 Moghaddam H and Hajirasouliha I (2008) Optimum strength distribution for seismic design of tall
473 buildings. The Structural Design of Tall and Special Buildings 17(2): 331-349.

474 Moghaddam H and Karami Mohammadi R (2006) More efficient seismic loading for multidegrees of
475 freedom structures. Journal of Structural Engineering ASCE 132(10): 1673-1677.

476 Motamedi M and Nateghi-A F (2008) A proposed lateral load pattern using seismic energy
477 distribution along the height of buildings. In *14th World Conference on Earthquake Engineering*,
478 Beijing, China.

479 Nabid N, Hajirasouliha I and Petkovski M (2017) A Practical Method for Optimum Seismic Design of
480 Friction Wall Dampers. Earthquake Spectra, In-Press. DOI: 10.1193/110316EQS190M

481 OpenSees (Open System for Earthquake Engineering Simulation) (2015) University of California,
482 Berkeley: PEER (Pacific Earthquake Engineering Research Center) See
483 http://opensees.berkeley.edu

484 Park K and Medina RA (2007) Conceptual seismic design of regular frames based on the concept of
485 uniform damage. Journal of Structural Engineering ASCE 133(7): 945-955.

486 PEER (Pacific Earthquake Engineering Research Center) (2010) PEER Ground Motion Database.

487 University of California, Berkeley, USA. See http://peer.berkeley.edu/smcat/search.html

488 Silva A, Daniello M, Rebelo C, Landolfo R, Simões da Silva L, Lima L (2016). High strength steel in
489 chevron concentrically braced frames designed according to Eurocode 8. Engineering Structures
490 124: 167-185.

491 SIMQKE (1976) A program for artificial motion generation, user's manual and documentation.
492 Vanmarke EH: Department of Civil Engineering, Massachusetts Institute of Technology,
493 Cambridge, USA.

494 Tenchini A, D'aniello M, Rebelo C, Landolfo R, Da Silva L, Lima L (2014). Seismic performance of
495 dual-steel moment resisting frames. Journal of Constructional Steel Research 101: 437-454.

496

497

498

499

500

501

502

503

List of Figures

List of Notations

D_t	Global damage index
h_i	Height from the base to level i
A_i	Shear distribution factor used in P.5 load pattern
C_B	Base shear coefficient used in P.5 load pattern
C_{iv}	Coefficient used in P.2 load pattern.
F_i	Lateral seismic force at ith storey level
F_t	The portion of the base shear that is applied as a concentrated force at the top of the structure
V_i	Storey shear force at level i
V_y	Base shear strength
V_{yi}	Shear strength of the ith storey
W_t	Total weight of the structure.
a_i, b_i, c_i, d_i	Constant coefficients corresponding to the soil profile used in P.3 load pattern
w_i	Total effective seismic weight of the structure located at i^{th} level
α_i	Coefficient used in P.5 load pattern
β_i	Shear distribution factor at level i
δ_{in}	Coefficient used in P.4 and P.9 load patterns
μ_T	Target ductility demand of structure
ξ_i	Coefficient used in P.7 load pattern
ϕ_i	Dimentional less parameter used in P.3 load pattern
b	Altitude of triangular load used in Iranian seismic code (BHRC, 2005)
c	Parameter to account for the plastic deformation magnitude
CP	Collapse prevention performance level of ASCE/SEI41-13
D_i	Cumulative damage index at ith storey
E	Elastic Modulus
E_T	Tangent Modulus
F_{ye}	Expected yield stress
I_b	Moment of inertia of the beam elements
I_c	Moment of inertia of the column elements

559	IO	Immediate occupancy performance level of ASCE/SEI41-13
560	l_b	Effective length of the beam elements
561	l_c	Effective length of the column elements
562	LS	Life safety performance level of ASCE/SEI41-13
563	MAE	Mean absolute error
564	Ms	Local magnitude of the earthquake
565	N	Number of plastic excursions
566	P	Axial force of the column
567	PGA	Peak ground acceleration of the earthquake
568	PGD	Peak ground displacement of the earthquake
569	PGV	Peak ground velocity of the earthquake
570	P_{ye}	Expected axial yield force of the column
571	R	Response modification coefficient
572	V	Total design lateral force at the base of the structure (base shear)
573	W_{pi}	Dissipated energy at i^{th} storey
574	Z	Plastic modulus of each cross-section
575	δ_{yi}	Nominal yield deformation of i^{th} storey
576	$\Delta\delta_{pj}$	Plastic deformation of i^{th} storey in j^{th} cycle
577	Θ_{all}	Maximum allowable rotation for life safety (LS) performance level
578	Θ_{pi}	Maximum plastic rotation of i^{th} element
579	Θ_{y}	Yield rotation specified in ASCE/SEI41-13
580	Ω_0	Overstrength factor
581	H	Total height of the structure from the base
582	T	Fundamental period of the structure
583	k	Coefficient used in P.4 load pattern
584	k	Exponent parameter related to the fundamental period of the structure
585	n	Number of storeys
586	α	Exponent parameter used in P.2 load pattern.
587	ϑ	Coefficient used in P.9 load pattern

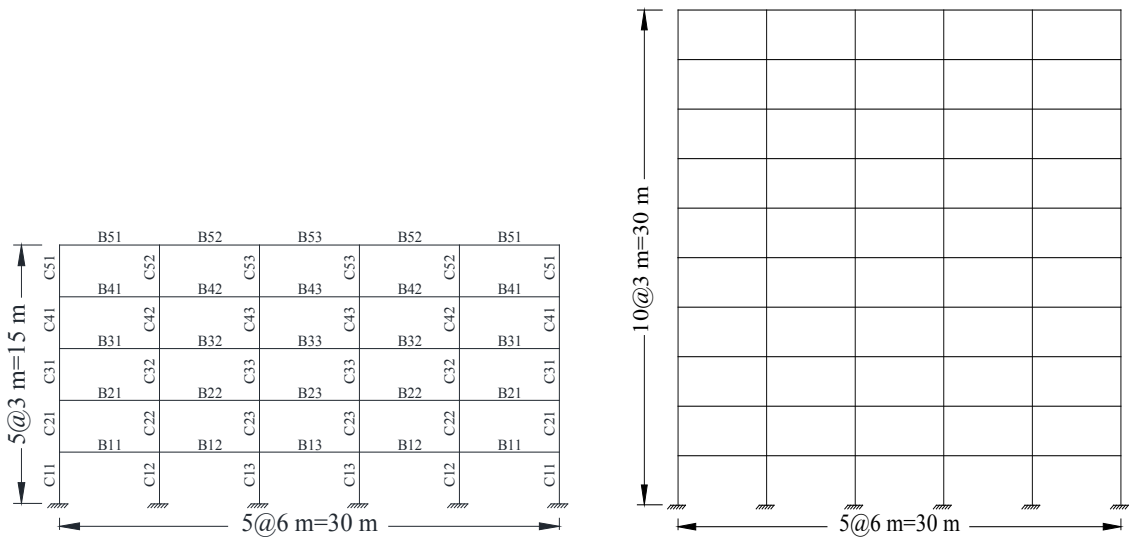

Figure 1. The schematic geometry of the 5 and 10-storey moment-resisting steel frames

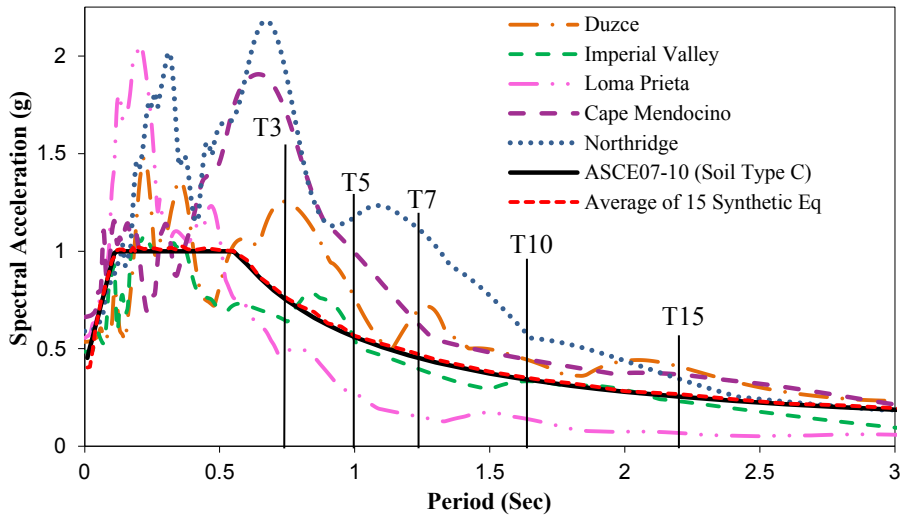

Figure 2. Spectral acceleration of the selected real earthquake records, average of 15 synthetic spectrum compatible earthquakes and ASCE/SEI 7-10 (T3 to T15 are first mode periods of the designed frames).

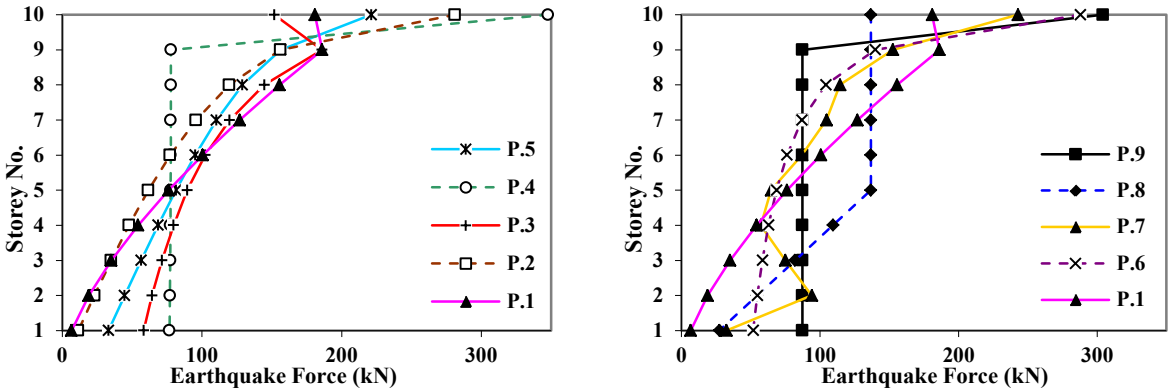

Figure 3. Lateral load patterns (P-1 to P-9) used to design 10-storey SMRFs

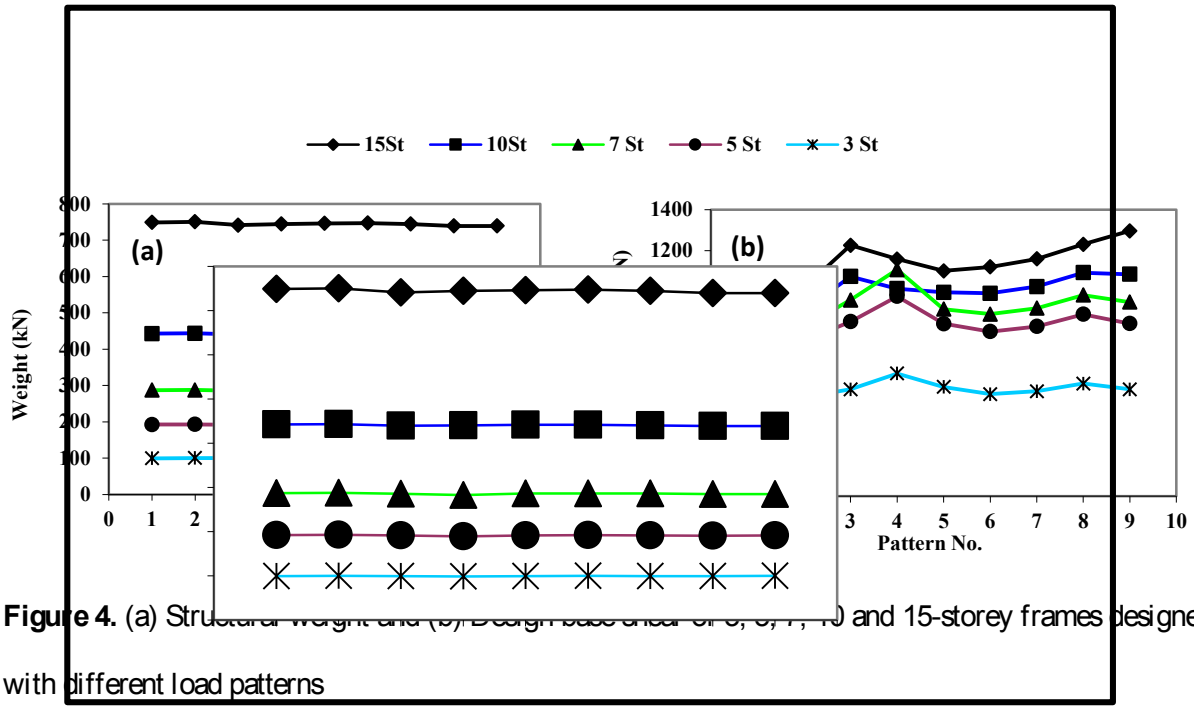

Figure 4. (a) Structural weight and (b) Design base shear of 3, 5, 7, 10 and 15-storey frames designed with different load patterns

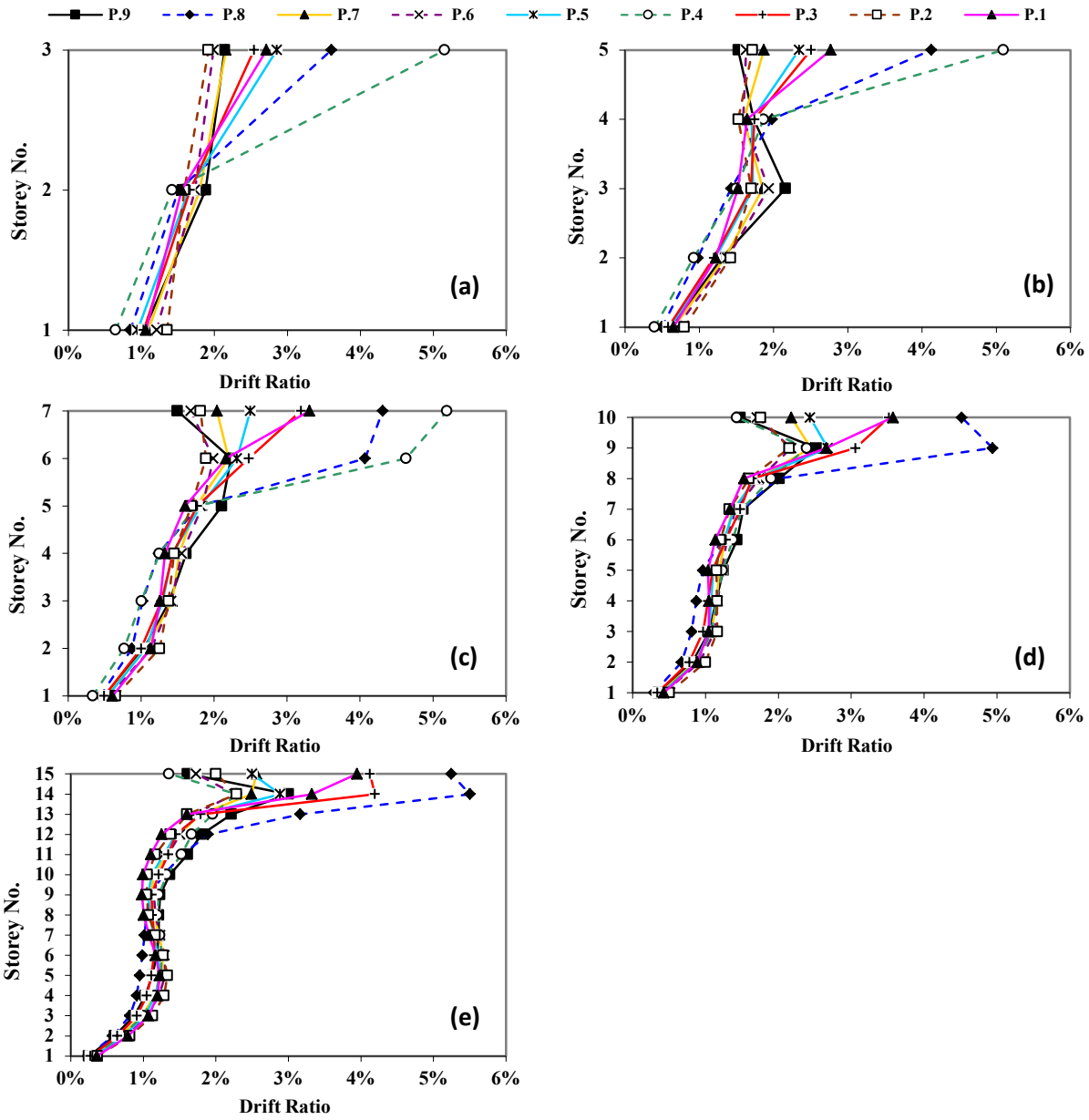

Figure 5. Average storey drift ratio of 3, 5, 7, 10 and 15-storey frames designed with different load patterns in 15 synthetic spectrum compatible earthquakes

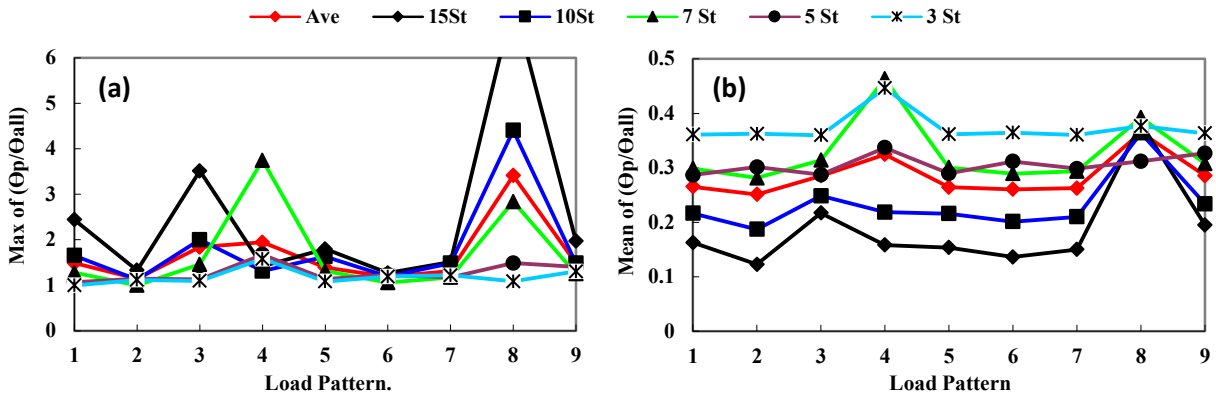

628

629 **Figure 6.** (a) Maximum (Θ_p/Θ_{all}), and (b) Mean (Θ_p/Θ_{all}) for the structural elements of the frames

630 designed with different load patterns, average in 15 synthetic spectrum compatible earthquakes

631

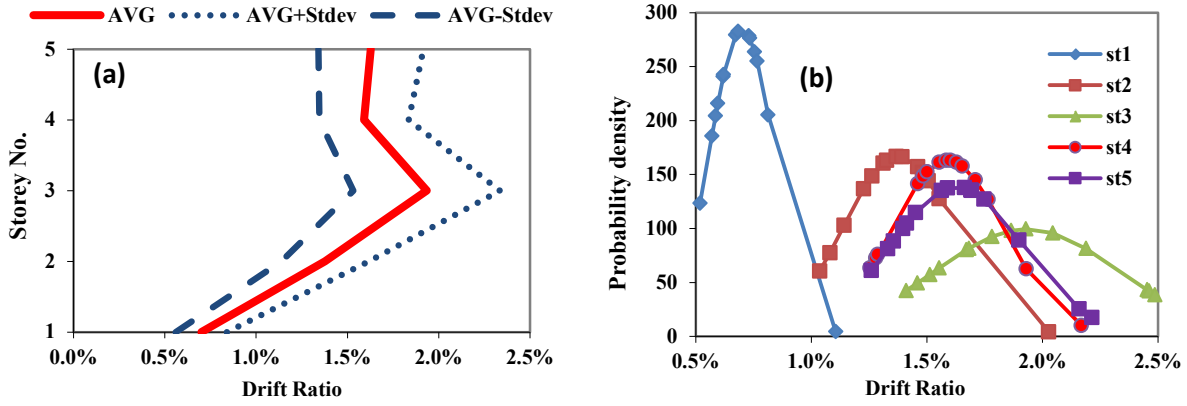

632 **Figure 7.** (a) Height-wise distribution of inter-storey drift ratios, (b) Probability density of maximum

633 inter-storey drift ratios, 5-storey frame designed with P-6 load pattern under 15 synthetic earthquakes

634

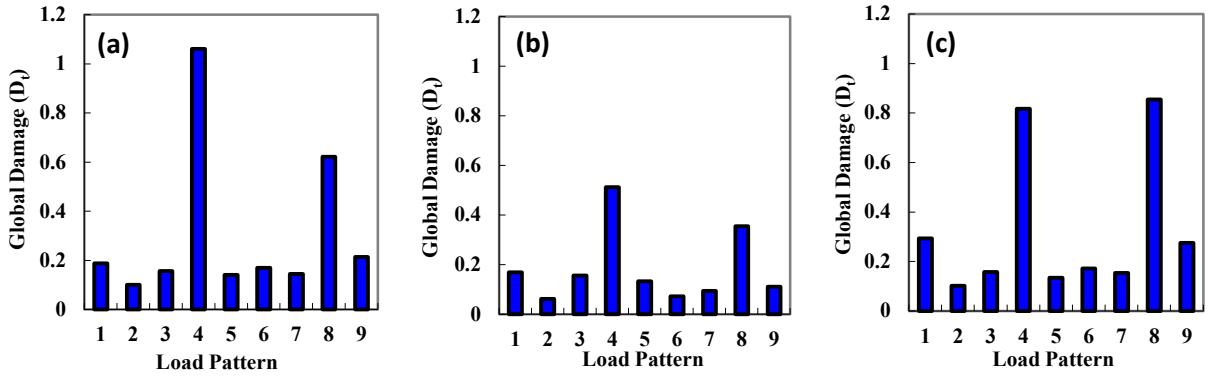

635

636 **Figure 8.** Global damage index of 5-storey frames designed with different load patterns under

637 synthetic spectrum compatible earthquakes (a) No. 4, (b) No. 8, and (c) No. 12

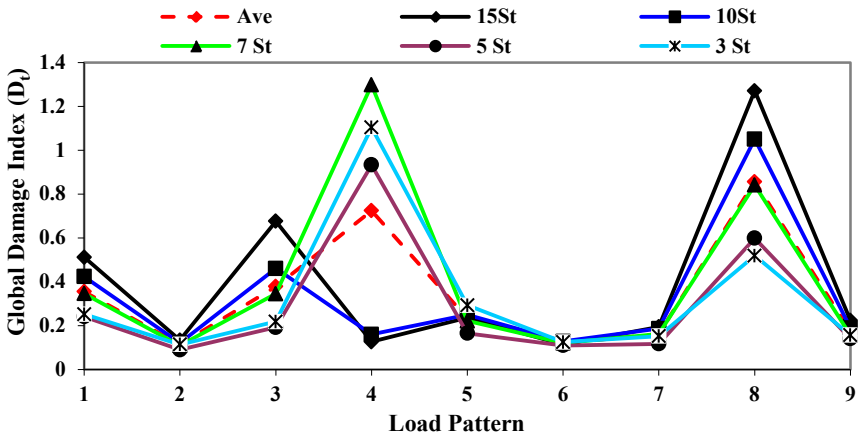

638

639 **Figure 9.** Global damage index of 3, 5, 7, 10 and 15-storey frames designed with the different load

640 patterns, average of 15 synthetic spectrum compatible earthquakes

641

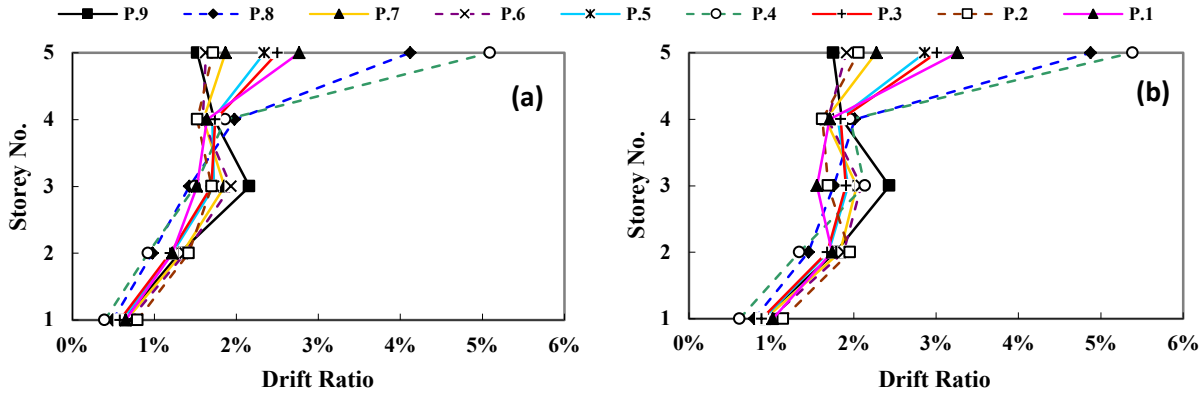

642 **Figure 10.** Maximum inter-storey drift distribution of 5-storey frames designed with different load

643 patterns (a) average of the 15 synthetic earthquakes, (b) average of the 5 real earthquakes

644

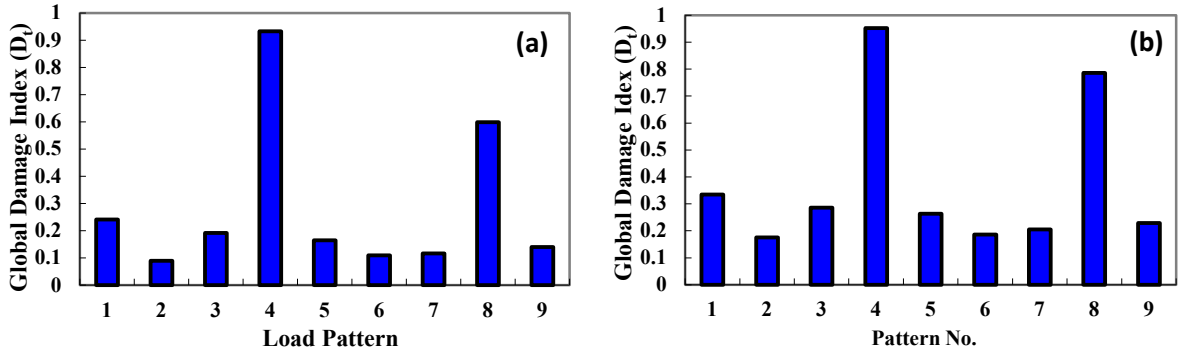

645

646 **Figure 11.** Global damage index of 5-storey frames designed with the different load patterns (a)

647 average of the 15 synthetic earthquakes, (b) average of the 5 real earthquakes

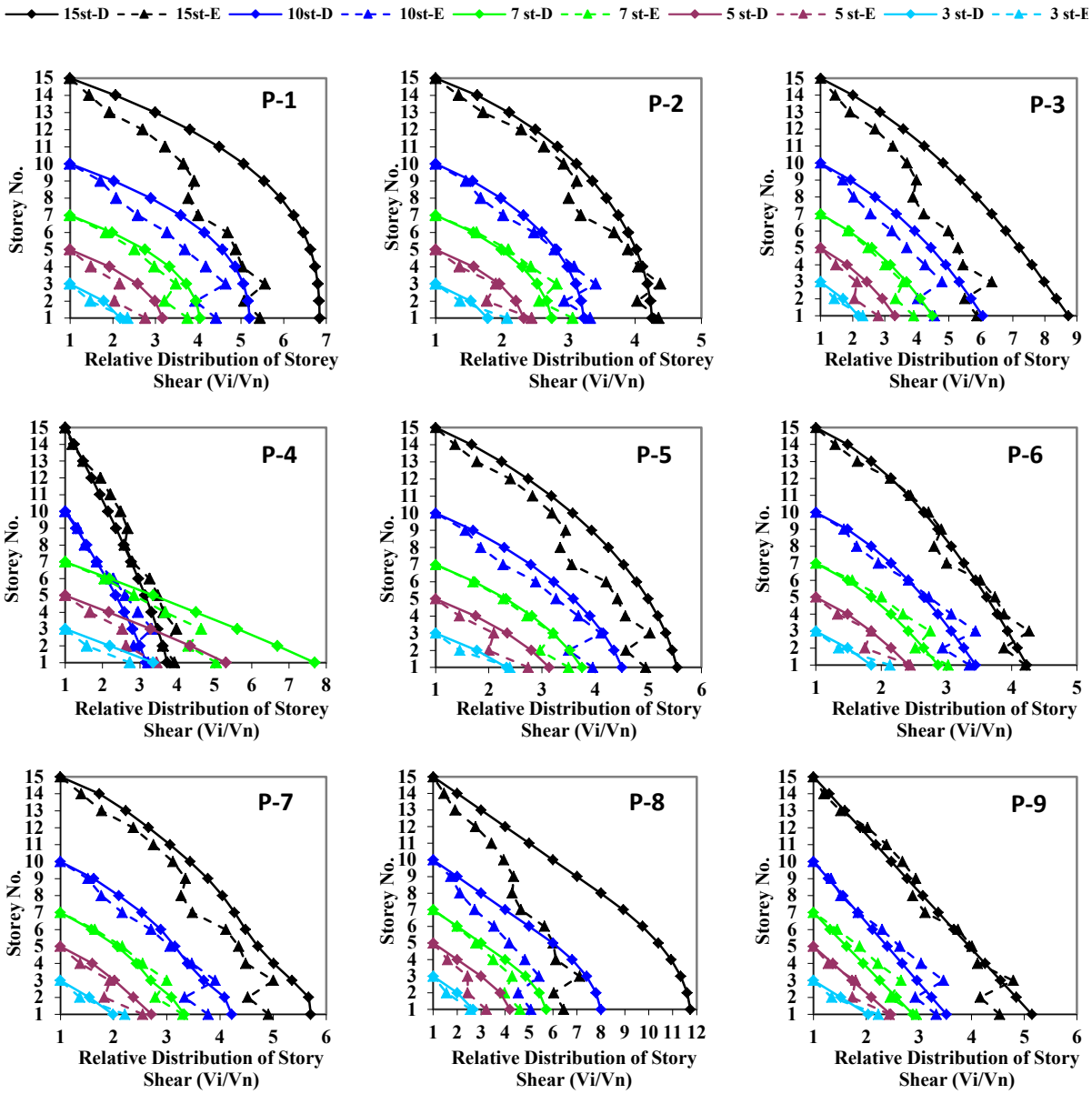

Figure 12. Comparison between the relative distribution of design storey shear forces and the average of storey shear forces exhibited in the 15 synthetic spectrum compatible earthquakes

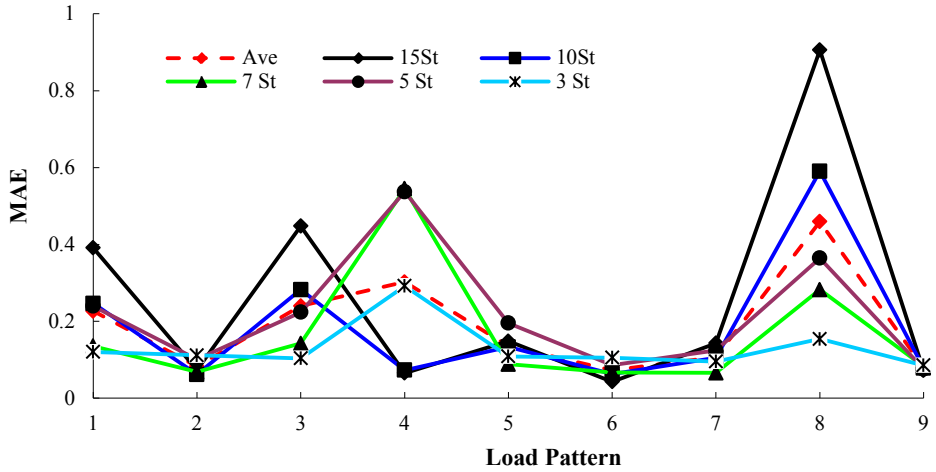

652

653 **Figure 13.** The mean absolute error (MAE) between $(V_i/V_n)_D$ and $(V_i/V_n)_E$ ratios for the 3, 5, 7, 10 and

654 15-storey frames designed with different load patterns